Journal of Colloid and Interface Science 652 (2023) 557–566

Contents lists available at ScienceDirect

Journal of Colloid And Interface Science

journal homepage: www.elsevier.com/locate/jcis

Controllable ingestion and release of guest components driven by interfacial molecular orientation of host liquid crystal droplets

Ruizhi Yang [a,1], Yueming Deng [a,1], Shuting Xie [a], Mengjun Liu [b], Yiying Zou [a], Tiezheng Qian [c], Qi An [a], Jiamei Chen [a], Shitao Shen [a], Albert van den Berg [d], Minmin Zhang [b,*], Lingling Shui [a,b,*]

[a] Joint Laboratory of Optofluidic Technology and Systems (LOTS), National Center for International Research on Green Optoelectronics, South China Academy of Advanced Optoelectronics, School of Information and Optoelectronic Science and Engineering, South China Normal University, Guangzhou 510006, China
[b] Guangdong Provincial Key Laboratory of Nanophotonic Functional Materials and Devices, School of Information and Optoelectronic Science and Engineering, South China Normal University, Guangzhou 510006, China
[c] Department of Mathematics, Hong Kong University of Science and Technology, Clear Water Bay, Kowloon, Hong Kong, China
[d] BIOS Lab-on-a-Chip Group, MESA+ Institute for Nanotechnology, Technical Medical Centre and Max Planck Centre for Complex Fluid Dynamics, University of Twente, AE, Enschede 7500, the Netherlands

GRAPHICAL ABSTRACT

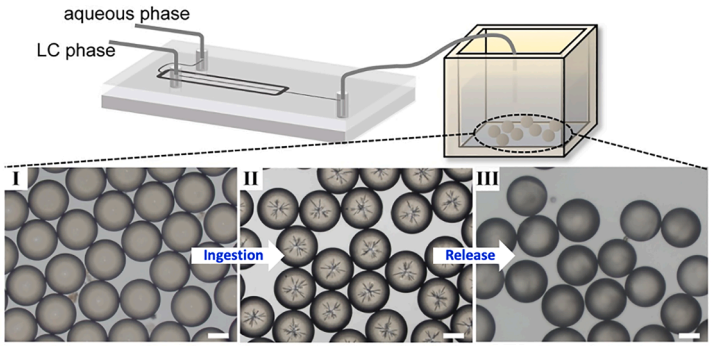

ARTICLE INFO

Keywords:
Liquid crystal
Nematic field
Topological defect
Self-assemble
Ingestion
Release

ABSTRACT

Controllable construction and manipulation of artificial multi-compartmental structures are crucial in understanding and imitating smart molecular elements such as biological cells and on-demand delivery systems. Here, we report a liquid crystal droplet (LCD) based three-dimensional system for controllable and reversible ingestion and release of guest aqueous droplets (GADs). Induced by interfacial thermodynamic fluctuation and internal topological defect, microscale LCDs with perpendicular anchoring condition at the interface would spontaneously ingest external components from the surroundings and transform them as radially assembled tiny GADs inside LCDs. Landau–de Gennes free-energy model is applied to describe and explain the assembly dynamics and morphologies of these tiny GADs, which presents a good agreement with experimental observations.

* Corresponding authors at: Joint Laboratory of Optofluidic Technology and Systems (LOTS), National Center for International Research on Green Optoelectronics, South China Academy of Advanced Optoelectronics, School of Information and Optoelectronic Science and Engineering, South China Normal University, Guangzhou 510006, China (L. Shui)
E-mail addresses: zhangminmin@m.scnu.edu.cn (M. Zhang), shuill@m.scnu.edu.cn (L. Shui).
[1] These authors contributed equally to this work.

https://doi.org/10.1016/j.jcis.2023.08.089
Received 14 April 2023; Received in revised form 15 July 2023; Accepted 12 August 2023
Available online 14 August 2023

Furthermore, the release of these ingested GADs can be actively triggered by changing the anchoring conditions at the interface of LCDs. Since those ingestion and release processes are controllable and happen very gently at room temperature and neutral pH environment without extra energy input, these microscale LCDs are very prospective to provide a unique and viable route for constructing hierarchical 3D structures with tunable components and compartments.

1. Introduction

Bottom-up and top-down are two widely used strategies for microfabrication [1–3]. As a bottom-up technique, droplet microfluidics is applicative for the massive and uniform fabrication of the multi-hierarchical structures, especially for soft matter systems [4,5]. But soft matter shows enormous response to even weak force and this therefore results in its poor capacity to resist deformation [6]. So, only relatively simple structures, such as packing model [7–9], could be produced when using droplet microfluidics with isotropous materials. To achieve multi-hierarchical structures with higher complexity, anisotropy material with sophisticated out-of-equilibrium architectures, complexity, adaptability, and responsiveness, such as liquid crystal, can be utilized to induce the formation of complex structure.

In 1997, Weitz et al. observed a two-dimensional self-assembly of water beads in the nematic field and explained the formation principle of this structure [10], which subsequently inspired Solodkov et al. [11] to generate similar fractal structures in LCD using mechanical shaking. After that, Guo et al. also used laser to induce the entry of an extra phase into LCD to generate fractal structure [12]. All these discoveries brought a new way for life sciences [13,14]. But they were unable to create these complex fractal structures using energy in very small magnitude, such as thermal fluctuations. So, in last decade, one fascinating research interest in this field is to explore the minimum energy level we could use to drive a soft matter system.

Herein, we present a spontaneous and reversible approach for controllable ingesting and releasing external components via the reorientation of LC molecules inside the LCDs, which is driven by switching the surfactant anchoring conditions at the LC-water interface. A microfluidic device is used to produce spherical nematic LCDs with well-defined size and high throughput. A radial alignment of the LC molecules would form inside each of these generated LCDs due to the initial homeotropic anchoring at the interface, and thus trapping the external components as tiny GADs which then assemble along with the local topological defects in the center of LCDs. The dynamics of this spontaneous assembly process can be explained by the Landau–de Gennes based free energy model and the theoretical calculation with this model shows a good agreement with the experimental observations. The resulting fractural structures of assembled GADs are configurable in the LCD by adapting the size of the host LCD and interfacial tension. When we used SDS as a typical surfactant for the experiment, the size of fractural structures increases with the decrease of interfacial tension and also with the increase of the host LCD's size. Besides, the active release of GADs from the host LCD to external medium was also investigated. When the LC molecular orientation at the LCD interface was changed from perpendicular to planar, GADs can be trigged to move towards the interface and eventually released. Since these processes could be triggered with very gentle and normal experimental conditions without intensive energy input, such tunable structures with submicron features over large areas of chemically accessible interfaces might be useful in the design of on-demand delivery systems with coupled chemo-electro-optical responses. It also mimics the intrinsic transmembrane movement of molecules/particles, which might be a potential model to mimic the endocytosis and exocytosis processes in nature and thus make artificial cells.

2. Results and discussion

2.1. Interfacial engineering of host LCDs driven by interfacial molecular orientation

The host LCDs with diameter range of 50–250 μm were generated using a droplet microfluidic chip in accordance with a well-established protocol [15]. Fig. 1**a** shows the schematic of the microfluidic device for preparing LCDs. The generated LCDs were collected and incubated in aqueous solutions containing sodium dodecyl sulfate (SDS) with different concentrations ranging from 5 mM to 360 mM. Theoretically, the concentration of SDS surfactant should be above the threshold concentration (1.3 mM) for the formation of homeotropic anchoring and the alignment of LC molecules at LC-water interface [16], and also be comparable to or higher than the critical micelle concentration (CMC) of SDS (8.9 mM) to assure the tight assembly of SDS molecules at the LC-water interface.

The ingestion and self-assembly processes of GADs are illustrated in Fig. 1**b**. When the LC molecules are homeotropically anchored at the interface of LCDs (Fig. 1**b (I)**), external components from the surrounding enter LCDs along the protrusion (Fig. 1**b (II) & (III)**) and then self-assemble as a radially structured GADs with a single point defect in the center of LCDs (Fig. 1**b (IV) & (V)**). Fig. 1**a (II)** shows a clear microscope image of ingested tiny GADs inside the LCDs with SDS aqueous solution environment. Reversely, when the anchoring direction is managed to planar anchoring at the LC-water interface, the GADs would be gradually released and empty bipolar LCDs with two surface points defects (or boojum) form, as shown in Fig. 1**c(V) & a (III).**

2.2. Spontaneous ingestion of GADs into LCDs

For GADs to enter LCDs, there must be some protrusions serving as breakthroughs at the LC-water interface. Normally, the protrusions can be induced by thermodynamic fluctuation. In our experiments, there was no additionally inputted external energy during the incubation process. So, we propose that at non-zero temperature, thermodynamic fluctuation generally affects all degrees of freedom of a system, allowing the system to randomly sample possible states with probabilities given by the Boltzmann distribution [17].

Thermodynamic fluctuation from the external aqueous surrounding would easily induce instabilities at the LC-water interface, especially with high surfactant concentrations. These instabilities would sequentially lead to protrusions at the LC-water interface, which forms a local concentration difference of SDS surfactant molecules and eventually facilitate the formation of small GADs, as illustrated in Fig. 2**a**. Moreover, the surface bending modulus exhibits high sensitivity to charge density. In our case, the charge density around LC-water interface is inhomogeneously distributed due to the presence of electric double layer and short-range protrusion interactions. Consequently, this uneven distribution of charges leads to the difference not only in interfacial tension but also in bending modulus, generating protrusions of small GADs at the interface with loose surfactants assembly. The protrusion frequency of a thermodynamically activated interfacial instability can be described by the Arrhenius equation written as $A_p \exp(-\Delta E/k_B T)$, where A_p is a protrusion frequency factor, k_B is Boltzmann constant, T is temperature in Kelvin, and ΔE is the temperature-independent energy barrier for activation.

In order to compensate the Brownian motion of surfactants in a

liquid environment, a thermodynamic fluctuation overcoming an energy barrier of 10 k_BT is required to produce a stable interfacial protrusion [18]. We expect the generation of a hemisphere-shaped protrusion with a radius of $a = \sqrt{10k_BT/2\pi\sigma} \approx 4$ nm, where we have used $T = 298.15$ K for the temperature and a typical interfacial tension σ of 2.33 mN/m for the SDS-laden LC-water interface. This scenario is highly reminiscent of an earlier work by Tseng and Prosperetti on interfacial instability [19]. They pointed out that the detachment of small GADs from the LC-water interface occurs at a local convergence point where the vorticity vanishes. In our case, such a convergence point can be created by thermodynamic fluctuation. The presence of surfactant molecules weakens the stabilizing effect of LC-water interfacial tension remarkably. This accelerates the growth of instability at the interface, resulting in protrusions.

A detailed schematic diagram showing the self-assembly of GADs is given in Fig. 2. Considering an initial nanodroplet of radius a, the elastic distortions generated by a volume of $\sim a^3$ are negligible, reducing the elastic energy by $\sim Ka^3/R^2 \sim 4 \times 10^{-21}$ J, where R is the radius of host LCD and K is a single elastic constant for splay, twist and bend deformations. This is just on par with the thermodynamic energy at 298.15 K, $k_BT = 4.2 \times 10^{-21}$ J. The elastic driving energy is not potent enough to drive small GADs towards the LCD's central defect and they remain at the edge of LCD. As a consequence, more and more nanodroplets present at the edge area with the time (Fig. 2**b (I)**). Once detaching from the LC-water interface, small GADs tend to coalesce into larger ones to reduce the surface energy until they reach a critical size of few micrometers (Fig. 2**b (I,II)**), at which the coalescence is prohibited by the orientational elasticity of LC nematic phase that forms a point defect (the black dot in Fig. 2**b (II)**). Herein, the role of thermodynamic energy is to bring small GADs together, causing them to interact and merge into larger microdroplets.

A similar phenomenon had previously been demonstrated by Loudet et al [20] that the elastic energy cost of the distortions of LCs around a single GAD of radius a scales with Ka, and the surface anchoring energy scales with Wa^2, where W is surface anchoring energy per unit area. Two distinct behaviors are expected depending on the scope of a. When a is smaller than K/W, the surface anchoring energy Wa^2 is weaker than the bulk elastic energy Ka. As a consequence, the small GADs do not induce distinct distortions of the LC phase (Fig. 2**b (I)**). Such GADs can freely diffuse and coalesce when they collide with each other. Different behaviors are observed when a is larger than K/W. The surface anchoring energy Wa^2 becomes dominant and the LC molecules adapt to a perpendicular orientation at the interface of GAD. Accordingly, LC distortions in the 3D LCD become noticeable, which results in the formation of GAD-defect dipoles (Fig. 2**b (II)**). The defect between neighboring GADs prevents them from further coalescence. Thus, the defect causes the segregation of the microdroplets. The global structure then forms dipolar symmetry and the defect between neighboring GADs prevents them from further coalescence (Fig. 2**b (III)**). The critical size of the GAD a is guided by the delicate balance between elastic and surface energies and is predicted to be of the order of 2 μm, based on a typical surface anchoring energy $W \sim 5 \times 10^{-6}$ J/m^2 and LC elastic constant $K \sim 10$ pN [12]. This estimated critical size is close to the experimental observations, providing a strong support to the described mechanism.

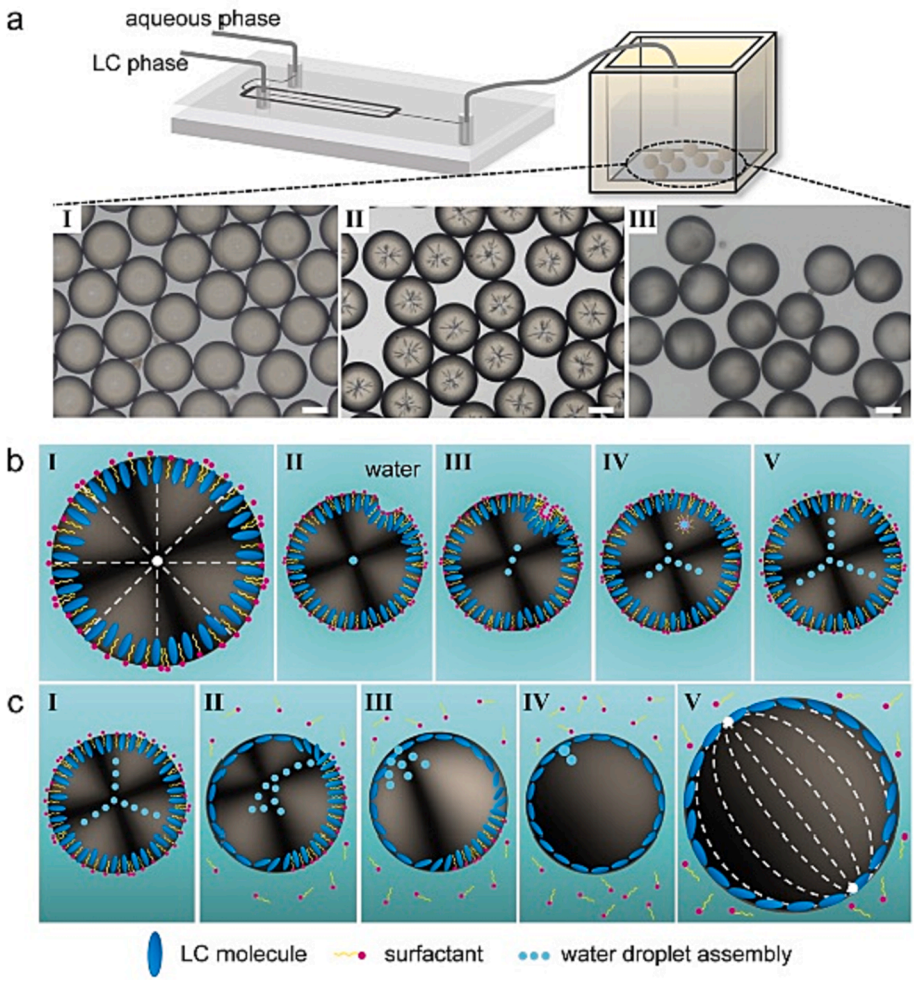

Fig. 1. Controllable ingestion and release of GADs driven by the interfacial molecular orientation of host LCDs. (**a**) Schematic illustration of a microfluidic device employed to generate monodisperse LCDs. The three optical images represent a complete process of ingestion and release of GADs through the LCDs: (I) freshly prepared LCDs, (II) self-ingestion and self-assembly of the medium phase in tiny droplets, namely GADs, and (III) release of GADs. Scale bars: 100 μm. (**b**) Schematic diagram of the self-assembly of complex inner structures and the alignment of surfactant molecules at the LC-water interface (white dash lines represent nematic director of LC and white dot represents the point defect). (**c**) Release of the assemblies formed by the GADs by tuning the point defect from the center to the boojum of the LCD. The inner structure moves from the center to the surface of the LCD, accompanied by the topological defect moving from the center towards the boojum.

2.3. Dynamics and spontaneous assembly of GADs confined in LCDs

When GADs near the LC-water interface grow large enough reaching $a \approx K/W$, they come to be mobile and move with acceleration toward the point defect in the center of the radial LCD (Fig. 3**a**). We used the simplest type of LC, nematic liquid crystal, which the average of LC molecules direction called the director $\hat{n}$, with the properties of $\hat{n}^2 = 1$ and $+\hat{n}$ being equivalent to $-\hat{n}$. Considering a nematic LCD with perpendicular boundary conditions and a topological point defect. In order to describe the interactions between these point defects, each one is assigned with a topological charge. A charge of +1 is assigned to the single point defect in the center of a radial LCD. As for the GAD-defect pair (Fig. 2**b (II)**), additional + 1 is assigned to the radial GAD, topologically compensated by a − 1 hyperbolic defect to form a dipole (analogous to an electric dipole) with a total topological charge of zero [21].

The motivation of GADs' movement can be explained by previously reported model: $x = (R^3 - 8\beta Kat/R_{\text{eff}}\eta)^{1/3}$ [12]. Here, x is defined as the displacement of a GAD from the center of the host LCD.$R = D/2$ is the radius of host LCD, β is the amplitude of the dipole director distortions determined by surface anchoring strength W, and K is the elastic constant in the one-constant approximation for splay, twist, and bend deformations, $R_{\text{eff}}\eta$ is the viscosity of the LC in the direction parallel to $\hat{n}$. Fig. 3**c** shows how the GAD's displacement x varies with time t. The theoretical dependencies are applied to fit the experimental trajectory to verify our model (blue curve). It is obvious that the model matches the experimental results well in our experiment conditions with $R =$ 60 μm, $a = 2$ μm, $R_{\text{eff}}\eta = 10$ mPa·s, and $K = 10$ pN. The only fitting parameter is $\beta = 0.21$, which is close to the value of 0.2 ± 0.02 for colloids modulated by patterned LC directors reported by Peng et al [22].

Based on the model, we propose the dynamics of GAD transportation and assembly processes as follows. Newly generated GADs with $a < K/W$ move slowly toward the center of the host LCD during the initial 14 s, as seen from the gradual slope in Fig. 3**c**. This is because, for a small nanodrop close to the edge of an LCD ($a \ll R$), the splay distortions created by a volume of $\sim a^3$ are negligible. The elastic driving energy does not provide enough power to take small GADs to the center defect of the LCD. When thermodynamic energy brings the small GADs together, they collide with each other and coalesce into bigger ones. Once the GADs grow up to $a \geq K/W$, LC distortions in the 3D LCD become significant, leading to the formation of GAD-defect dipoles. The +1 defect in the center of the radial LCD (host) attracts the −1 hyperbolic defect of the GAD-defect dipole, resulting in a migration of the GADs towards the center of the host LCD. As a consequence, the GAD-defect dipole is driven toward the LCD center, as seen from the model-experiment comparison in Fig. 3**c**.

At moderate surfactant concentration, the colloidal GADs with homeotropic anchoring at the GAD's interface first gather into linear chains by analogy with electrostatics. The GAD-defect dipoles behave like electrostatic dipoles at long range, resulting in the formation of chain-like structures in which the dipolar GAD-defect assemblies are pointing in the same direction (Fig. 2**b (III)**). The presence of a topological defect between two neighboring GADs produces a short-range repulsion that prohibits them from getting too close, thus inhibiting their further coalescence. In a pure splay pattern, the resultant GAD chains preserve their orientation along the radial alignment direction of the LC molecules.

Fig. 3**b** illustrates the assembling process of GADs and their corresponding fractal structures with linear chains extending radially outward from the center of the host LCD since the two adjacent chains repel each other. This suggests that there are some specific fractal structures with symmetry to minimize the elastic distortion energy. One example is the fractal structure at $t = 1$ h, a flat triangle frame was formed with the angle between the neighboring chains being $120^\circ \pm 5^\circ$. A tetrahedral frame is then obtained as time increases to $t =$ 64 h, similar to the phenomenon demonstrated by Solodkov et al. [11] That is, under the 3D symmetry balance, the tetrahedral configuration is the structure with the lowest order. As more GADs moved toward the core of the LCD, the branches of the fractal patterns extended and split (Fig. 3**b** at $t = 128$ h). Guo et al. explained that, as the size of fractal structure increases, the accessible surface area becomes larger and there is more available space for the assembling of mutually repelling GADs [12]. The diameter of the fractal structures d is plotted as a function of t in Fig. 3**d**. A steady state with d staying at around 125 μm was achieved based on a typical host LCD with R ~100 μm and the SDS concentration $c \sim$ 90 mM. These fractal structures remained stable for at least a week due to the stabilizing effect of topologically imposed hyperbolic defects separating the neighboring GADs.

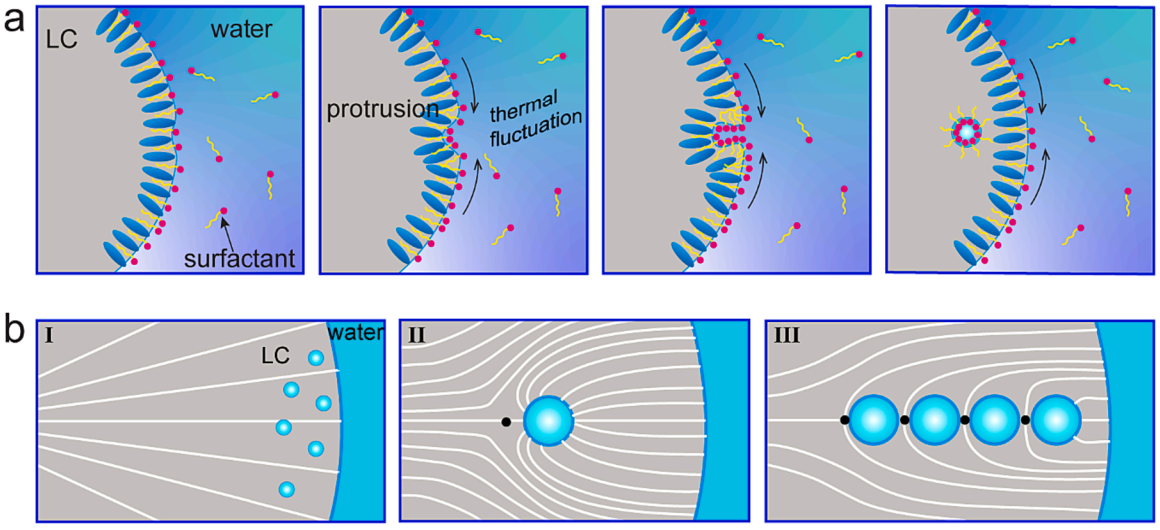

Fig. 2. Schematic of ingestion, merge and assembly of GADs in an LCD. (**a**) Schematic diagram of a plausible ingestion scenario caused by thermodynamic fluctuation. The arrangement of liquid crystal molecules and surfactant molecules at the LC-water interface is illustrated. (**b**) Schematic drawing of the director field in the LCD after GADs ingestion. White lines represent the nematic director of LC. (I) The GADs in nanometer size cannot cause distinct distortions of LC medium until they collide and merge into larger drops. (II) The coalescence of neighboring nanodroplets is prevented by the point defect (represented by the black dot) and a critical size of GAD is reached. The homeotropic order of nematic LC molecules around a GAD shows the symmetry of a dipole type. (III) Linear assembly of dipolar GADs and their further coalescence is prohibited by the formation of a defect between neighboring GADs.

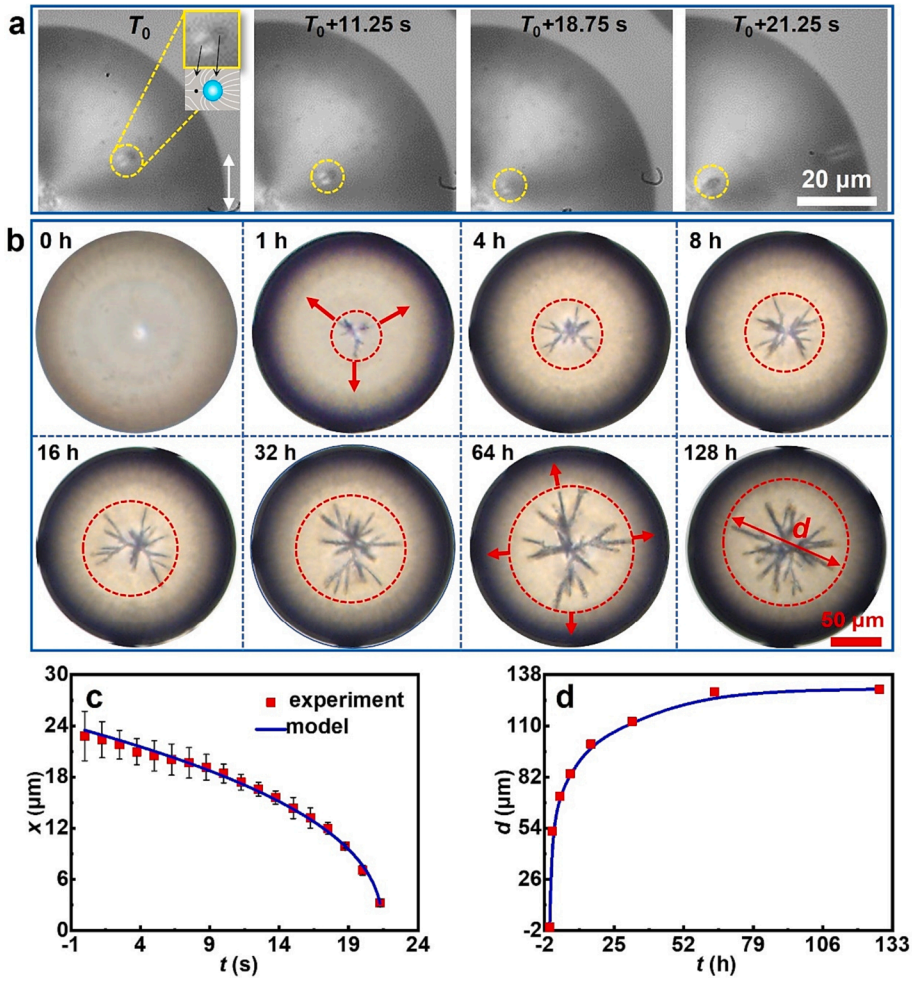

Fig. 3. Dynamics of the GADs confined in an LCD. (a) Dynamics of a GAD in time sequence. (**b**) Assembly of GADs in a host LCD dispersed in 90 mM SDS aqueous phase. The GADs form fractal structures and extend toward the interface. (**c**) Displacement of GAD × as a function of time, which are measured from the images in (a). (**d**) Corresponding diameter of fractal structures (red circles in (b)) ***d*** as a function of time.

2.4. Regulation for the size of GADs fractal structure in LCDs

The Landau–de Gennes based free energy model [23] is applied here to understand the physics behind the spontaneous assembly and identify the influence of the interfacial tension and sizes of LCD on the resultant fractal structures. In this model, the competition between the bulk elastic energy due to deformation and the local variations of the degree of order are considered: the volumetric contributions from the short-range Landau-de Gennes bulk free energy F_L and the long-range elastic free energy F_E, and the surface contributions from the surface anchoring energy F_S. Both F_L and F_E scale with $R^3(F_V = F_L + F_E)$. Whereas $F_S = -\frac{1}{2}W\int dSsin^2\Phi$, where Φ is the angle between the LC director ($\hat{n}$) and the preferred orientation of LC at the interface. For a radial configuration induced by surfactants, there is no contribution from the surface anchoring energy as the preferred orientation of LC at interface is parallel to $\hat{n}(\Phi = 0)$. So, the surface term, that is the interfacial free energy $F_\sigma = -\sigma\int dS$, describes the influence of surfactants on the free energy of the system (See Calculation Details). Sequentially, the total free energy F is defined as $F = F_V + F_\sigma$. Since interfacial tension plays a role in F_σ and LCD size also plays a role in both F_σ and F_V , so, by changing the types and concentrations of surfactant and the size of LCD, we could control F, therefore, also the size of resultant fractal structures.

2.5. Optimization of interfacial tension for spontaneous GADs assembly

Different types and concentrations of surfactant were used to investigate the effect on structural configurations of assembling GADs in this part. The interfacial tension of surfactant-laden LC-water interface is measured to be 0.17, 2.33 and 9.70 mN/m, respectively for cationic surfactant CTAB, anionic surfactant SDS, and nonionic surfactant TWEEN 20 at 10 times CMC (to ensure a stable perpendicular anchoring at the LC-water interface). In CTAB solution, the stable host LCD with diameter D above 60 μm is difficult to produce due to its low interfacial tension. Meanwhile, the spontaneous assembly of GADs happens quickly at the early stage of the incubation of the host LCD of D ~41 μm, being difficult to identify the dynamics of the self-assembly process as shown in Fig. 4**a**. When TWEEN 20 is applied, the assembly of GADs can be observed only in large host LCD with $D \geq 212$ μm (Fig. 4**b**). These factors limit the investigation and the spectrum of the assembly process, thus the construction of fractal structures. In contrast, SDS allows us to create LCDs in a much wider size range and to construct a rich spectrum of complex architectures, including those of lower order in Fig. 4**c** and higher order in Fig. 4**d**. A comparison of these three representative surfactants is summarized in Fig. 4**e**, in which SDS is shown to be the optimal choice.

Fig. 5**a–e** present the formed fractural structures of GADs in LCDs with D ~ 200 μm after incubating for 128 h in SDS solutions with concentrations of 5, 8.9, 89, 178 and 356 mM, and as summarized in Fig. 5**g, a** clear size increase of the fractal structure is shown, ranging

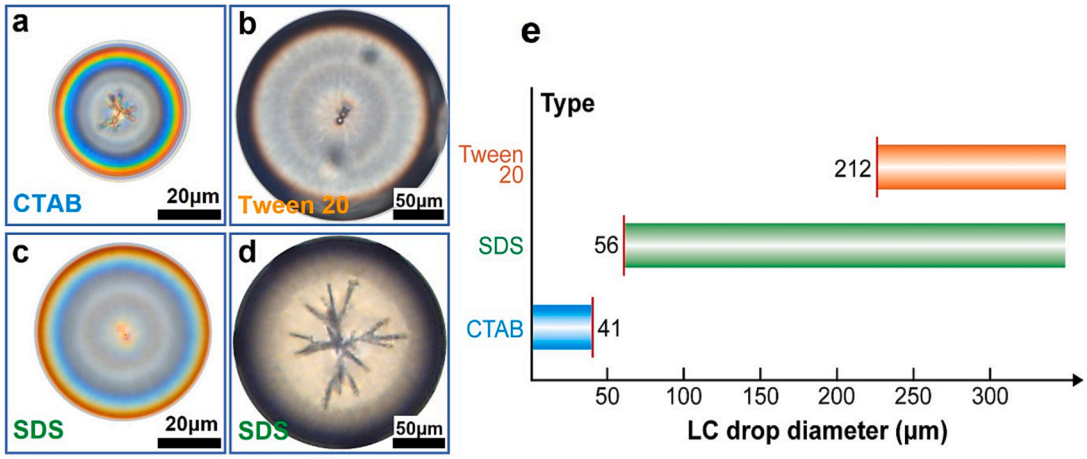

Fig. 4. Optimization of surfactant type. (**a**) A representative LCD (D ~41 μm) produced using a 9.2 mM CTAB aqueous solution as the outer phase. (**b**) A representative LCD (D ~212 μm) produced using a 0.6 mM Tween 20 aqueous solution as the outer phase. (**c-d**) Representative LCDs produced using a 89 mM SDS aqueous solution as the outer phase, showing low and high order fractural structures in a small and large LCD, respectively. (**e**) Comparison of the achievable LCDs using the three surfactants.

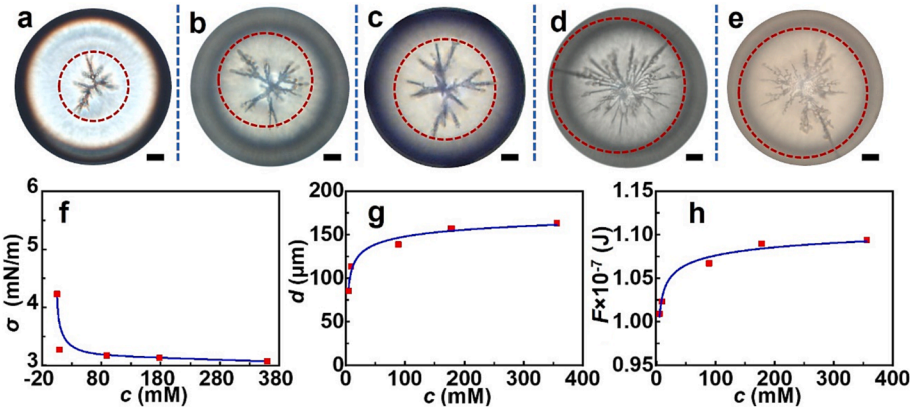

Fig. 5. Effect of SDS surfactant concentration on the configuration of GADs. (**a-e**) Spontaneous assembly of GADs confined in an LCD with D ~200 μm by incubating in SDS aqueous solutions at various concentrations of 5 mM, 8.9 mM, 89 mM, 178 mM and 356 mM, respectively. (**f**) Interfacial tension of the LC-water interface as a function of SDS concentration. (**g**) The fractal structure size d indicated in (a-e) as a function of SDS concentration. (**h**) The free energy of the system F as a function of SDS concentration. Scale bars in (a-e): 20 μm.

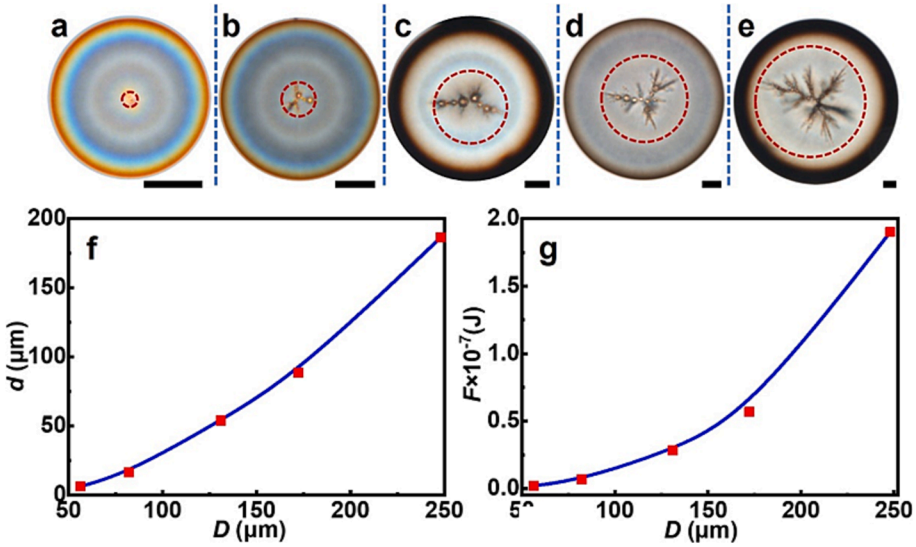

Fig. 6. Effect of LCD size on the configuration of GADs. (**a–e**) LCD with diameter of 56 μm, 82 μm, 131 μm, 172 μm and 248 μm, respectively, incubated in 8.9 mM SDS aqueous solution. (**f**) The fractal structure average d as a function of LCD's diameter D. (**g**) The free energy F with respect to LCD's diameter D. Scale bars: 20 μm.

from 82 to 168 μm. However, above a critical micelle concentration of 8.9 mM, the interfacial tension becomes essentially constant, as shown in Fig. 5**f**. The SDS concentration directly affects W, and thus influences the critical size of GAD (K/W) and also the corresponding fractal structures. Nevertheless, a higher SDS concentration leads to a higher W that results in smaller building block size a with denser fractal structure in Fig. 5**e**.

2.6. Effect of LCD size on the spontaneous GADs assembly

As noted above, available space for GADs assembly also influences the inner configurational architectures. We therefore feature the role of the LCD size in the assembly process and the corresponding results. We expect the ultimate fractal structures to be remarkably dependent on the host LCD size since the volumetric energy term F_v scales with R^3 and the surface term scales with R^2. We thus predict the free energy F, which is the difference of volumetric term outweighs surface term, to increase monotonically with LCD size.

We hence characterized the assembly of GADs within different size of LCDs while keeping the surfactant type and concentration constant. We found that the order of the fractal structure increases as the size of LCD grows (Fig. 6**a–e**). This is demonstrated in Fig. 6**f** that the average d of the fractal structure rises significantly from 6 μm to 186 μm when the diameter D of LCDs change from ~56 μm to ~248 μm.

To further confirm the prediction, F is calculated and presented in Fig. 6**g**. As expected, a similar trend to the evolution of the size of fractal structure is obtained, verifying the validity of our model.

The LC-water interface is coupled with the director field through the anchoring condition at the interface. For a small LCD (Fig. 6**a**), this coupling is strong due to the large elastic distortion of director field ($\nabla \bullet \hat{n} \propto 1/r$). Consequently, interfacial fluctuation and intake of nano-scale GADs are largely suppressed. Furthermore, it takes space and time for small GADs to undergo random motion and coalesce into large ones (for dipole formation). Therefore, only a small number of GADs can undergo coalescence near the center of the LCD, where director field undergoes extreme distortion. As a result, dipolar configuration of GAD-defect pair is energetically very expensive, and hence unlikely to form near the center of the LCD. This is why the fractal structure does not grow at all in small LCDs.

Taken together, the assembly of configurational architectures inside a radial LCD can be precisely controlled and manipulated by adjusting the interfacial tension, and also the size of the host LCDs.

2.7. Reconfiguration and release of GADs

In application such as on-demand delivery, the release of GADs is highly important. So, except for the ingestion control, we have also investigated the release of ingested GADs from the LCDs. Recently, several studies have reported the on-demand release of guest droplets from nematic liquid crystals. Y. Kim et al. investigated the release of guest aqueous microdroplets into the external aqueous solution from flat Liquid Crystal (LC) films driven by a propagating nematic (N) to an isotropic (I) interface across the LC as the LC undergoes the N-I phase transition [24]. The N–I phase transition was achieved by contact heating. Furthermore, P. Beyazkilic et al. developed a guest aqueous microdroplet release system based on near infrared (NIR) light excitation using photothermal dye-doped nematic LC. LC undertook a N–I phase transition due to the photothermal heating by illuminating an NIR laser on the LC surface [25]. In another work, J. Guo et al. conducted the release of a guest droplet from a liquid crystal droplet induced by locally heating the host LC [12]. In this study, we aim to identify the minimum energy level required to trigger a release in a nematic LC system. Contrary to the above referred studies that require additional energy to achieve N–I phase transition, our release system only depends on the anchoring condition at the water-LC interface without any extra energy input. The release process was achieved by controlling the LC molecular orientation from perpendicular to planar at the host LCD's interface, which is able to be manipulated by the interfacial anchoring conditions of surfactant molecules.

It has been reported that the perpendicular anchoring at the LC-water interface can be achieved at high SDS concentration above 600 μM [16]. Jake Shechter et al. have also found the radial to bipolar structural transition of LCDs occurs when the SDS concentration is below 600 μM [26]. LCDs with diameter of 200 μm were generated and dispersed in an 89 mM SDS aqueous solution. 20 μL LCDs aqueous dispersion was transferred into a glass container. The dispersion then was diluted by quickly adding 5 mL DI water, making the final SDS concentration in aqueous phase to be 178 μM, much lower than the above-mentioned concentration for perpendicular anchoring. As a result, SDS molecules start to depart from the LC-water interface and diffuse into the bulk aqueous solution, and this process is accompanied by the switching of interfacial anchoring direction. Meanwhile, the +1 defect in the center of the radial LCD starts to escape from the center toward the pole (boojum) of the spherical LCD. This defect movement drives the GADs to move toward the interface and eventually expel them from the host LCD. As soon as the released GADs get into contact with the bulk aqueous solution at the interface of LCD, they would quickly dissolve back to the aqueous phase. Fig. 7**a** and **Figure S1** present the detailed step-by-step process captured under polarization optical microscopy (POM) and normal optical microscopy (OM), respectively. The corresponding dynamic releasing process is analyzed in Fig. 7**b**, reflecting a mirror trend compared to the self-assembling process of Fig. 3**d**. However, the time scales are noted to be very different. Fig. 3**d** shows that d grows slowly in a stationary director field, while Fig. 7**b** shows that d decreases quickly in an evolving director field.

To prove the viability of this process, we have also replaced SDS with PVA (a planar anchoring surfactant) and found a similar phenomenon. The OM results and POM results showing the detailed release process of GADs are presented in **Figs. S2a and S2b**, respectively. The releasing speed is slower than the dilution process addressed above due to the slow diffusion of PVA molecules compared to SDS molecules.

To validate that such a release process is controlled by the splay energy and the position change of the point defect from center toward boojum of the host spherical LCD due to reorientation of the LC molecules at the LCD's interface, we have also increased the temperature above the nematic-isotropic phase transition temperature (T_{NI}) of 35.5 °C to eliminate the point defect. As shown in **Figure S3**, when the temperature increased to 35 °C, which is slightly lower than T_{NI}, although the small GADs moved toward each other and merged into a single larger GAD, the larger GAD was still in center of the LCD due to nematic confinement of the central point defect, without escaping towards external environment. When the temperature was higher than T_{NI} and the LCD is in the isotropic phase, the topological defects that stabilize the GADs disappear, and hence the GADs moved around and become randomly distributed, but still stayed inside the LCD. These results further prove that the point defect in the LCD is essential to capturing and leading the assembly and motion of GADs. Moreover, this process tells us that the LCD can indeed function as a smart device/machine actuated by the molecular alignment at the interface which can be stimulated by the interfacial properties and the environmental conditions.

2.8. On-demand delivery using LCDs

Controlled uptaking and loading biochemicals with precise volume fraction in carrier microdroplets, and triggered on-demand releasing are highly desired in the development of drug and pharmaceutical nutrient delivery systems. Thus, in the last part of this work, we investigated the potential of 3D LCD system in on-demand delivery. Based on the remarkable phenomenon we observed, we employed a fluorescence dye as a representative substance mimicking the ingestion and release

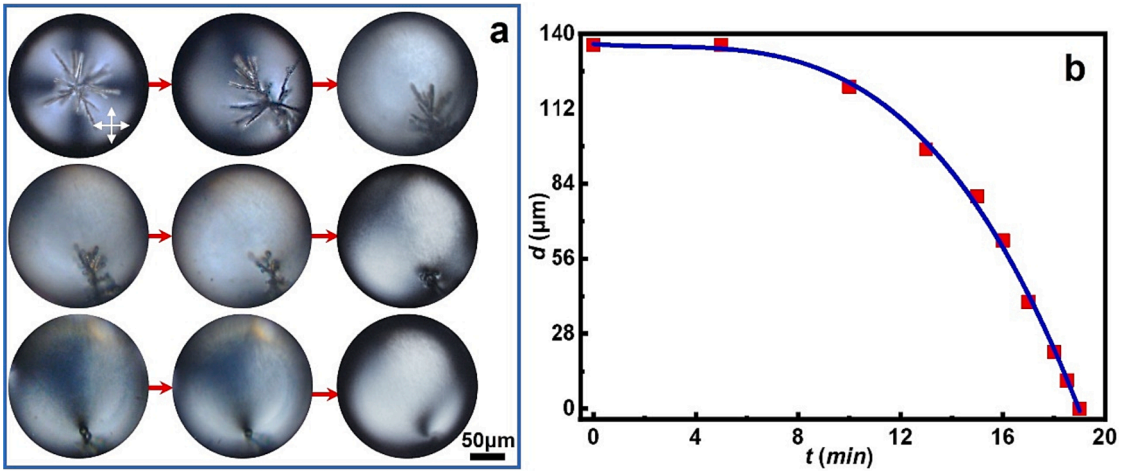

Fig. 7. Controlled release of GADs from an LCD. (**a**) POM images showing the release process of GADs from a host LCD. (**b**) The size of the fractal structure *d* as a function of time *t*.

processes of carrier for proof-of-concept demonstration. We employed fluorescein sodium salt as a representative target substance and the LCDs as carriers. The process was visualized by fluorescence microscopy. As shown in **Figure S4**, the same ingestion and release behavior as demonstrated in Fig. 3 and Fig. 7, respectively, were observed. When LCDs of 130 μm were dispersed in a mixture of 89 mM SDS aqueous solution and 12.7 mM fluorescein sodium salt aqueous solution, ingestion of GADs containing fluorescein sodium salt occurred spontaneously, leading to the formation of fractural structures of fluorescein-GADs (**Figure S4a**). The assembly was released by quickly adding 3 mL of DI water, actively transporting fluorescein-GADs from the interior to the exterior of the LCD (**Figure S4b**). The ingestion and release behavior could be easily controlled by the anchoring condition of LCs at the interface of LCDs. Compared with most existing microdroplet carriers, the high throughput preparation, room temperature operation, no energy input, precise manipulation, highly controllable performance and fast response are the advantages of the LCDs.

3. Materials and methods

3.1. Materials

4-pentyl-4′-cyanobiphenyl (5CB, 99 %) was obtained from J&K Scientific Ltd. (Beijing, China), while hexadecyltrimethylammonium bromide (CTAB ≥ 98.0 %), Tween 20, fluorescein sodium salt, polyvinyl alcohol (PVA, average molecular weight 130 k) and sodium dodecyl sulfate (SDS ≥ 98.0 %) were purchased from Sigma-Aldrich (Shanghai, China). DI water (18.25 MΩ at 25 °C) was prepared using a Milli-Q Plus water purification system (Milli-Q Plus water purification, Sichuan Wortel. Water Treatment Equipment Co. Ltd, Sichuan, China).

3.2. Preparation of LCDs using microfluidic device

The inner LC phase is sheared off by the outer aqueous phase at the flow-focusing area to form monodispersed LCDs in micrometer size. The size of the LCDs can be tuned by employing different shear openings. Herein, we use a 15 μm shear opening for generating LCDs with diameter in the range of 20–80 μm; while we use a 50 μm shear opening for preparation of LCDs with diameter larger than 80 μm. Two types of glass microfluidic chips (FFDG.2/FFDG.2.5, Micronit Microfluidics, Enschede, the Netherlands) with flow-focusing geometry were used to prepare LCDs. The size of LCDs can be controlled by applying different shear openings. We use 15 μm shear opening for producing LCDs of diameter 20–80 μm, and 50 μm shear opening for formation of LCDs of diameter larger than 80 μm. Liquid crystal (5CB) was used as an inner phase, whereas aqueous solution with surfactants (SDS, CTAB or Tween 20) were used as an outer phase. The inner phase was sheared by outer phase to form uniform LCDs. The generated LCDs are collected in a container filled with SDS aqueous solution. The resultant LCDs were collected in a container with a glass cover to prevent the emulsion from volatilization.

3.3. Release of inner fractal structures

20 μL of LCDs stabilized by 89 mM SDS with intricate fractal structures were prepared and stored in a glass container. To dilute the emulsion, 5 mL of DI water was rapidly added. For the PVA solution-induced release, 1 mL of PVA (3 %, w/w) was quickly introduced into the LCD emulsion without any additional excessive operations.

3.4. Fluorescence microscopy imaging

LCDs with 130 μm were generated and dispersed in an 89 mM SDS aqueous solution containing fluorescein sodium of 12.7 mM. A glass container was employed for collecting the generated LCDs. Fluorescent microscope (Olympus, IX73, Tokyo, Japan) mounted with a 100 W lamp (Olympus, USH-1030L) as an excitation light source and a digital camera (Olympus, DP73, Tokyo, Japan) for image acquisition was used to visualize and image the spontaneous ingestion and release process at several representative moments. The samples were exposed to a laser with an excitation wavelength of 480 nm.

3.5. Characterization

Generation of host LCDs was monitored using an inverted optical microscope (Olympus IX2, Tokyo, Japan) equipped with a high-speed camera (Phantom, MIRO MIIO, Vision Research Inc., Wayne County, NC, USA) in the FF illumination mode. Polarized optical microscopy (POM) and optical microscopy (OM) images of the host LCDs were captured by an inverted microscope (Olympus IX73, Tokyo, Japan) in the FF mode matched with a digital camera (Olympus DP73 camera, Tokyo, Japan). For dynamics of confined GADs inside a host LCD, an inverted microscope (Olympus IX73, Tokyo, Japan) with a high-speed camera (Phantom, MIRO MIIO, Vision Research Inc., Wayne County, NC, USA) in analysis mode was employed to capture the detailed movements.

3.6. Calculation of free energy

Herein, we describe our model based on the free energy calculation

which is comprised of volumetric contributions from Landau-de Gennes bulk free energy and elastic free energy, and surface contribution from surface anchoring energy. An additional surface term so-called interfacial free energy that describes the effect of interfacial tension on the free energy of the system is included in our model.

The reorganization of LCDs is described with a continuum model for the free energy of the material in terms of the tensorial order parameter of the LC, $\boldsymbol{Q}$, defined as [23]:

$$\boldsymbol{Q} = \frac{3}{2}\mathbb{S}\left(\hat{\mathrm{n}}\hat{\mathrm{n}} - \frac{1}{3}I\right) \tag{1}$$

where $\mathbb{S}$ is the scalar order parameter, $\hat{\mathrm{n}}$ is the director field, and I is the identity matrix. The free energy F is the sum of volumetric term and surface term [27]

$$F = F_{\mathrm{L}} + F_{\mathrm{E}} + F_{\mathrm{S}} \tag{2}$$

where F_{L} is Landau-de Gennes bulk free energy, F_E is elastic free energy, and F_S is surface free energy.

The Landau-de Gennes bulk free energy can be expanded by $\mathrm{Tr}(\boldsymbol{Q})$ [23]:

$$F_L = \int dV\left[\frac{A}{2}\left(1 - \frac{U}{3}\right)Tr(\boldsymbol{Q}^2) - \frac{AU}{3}Tr(\boldsymbol{Q}^3) + \frac{AU}{4}Tr(\boldsymbol{Q}^2)^2\right] \tag{3}$$

where parameter A denotes the energy density scale and U is a temperature dependent dimensionless constant. The parameters used here are: $A = 1.17 \times 10^5\ \mathrm{J{\cdot}m^{-3}}$ and $U = 5$ [23].

The elastic free energy F_S can be expressed as [28]:

$$F_E = \frac{1}{2}\int dV\left\{K_{11}(\hat{\mathrm{n}}\nabla{\cdot}\hat{\mathrm{n}})^2 + K_{22}(\hat{\mathrm{n}}{\cdot}\nabla\times\hat{\mathrm{n}})^2 + K_{33}[\hat{\mathrm{n}}\times(\nabla\times\hat{\mathrm{n}})]^2\right\} \tag{4}$$

where K_{11}, K_{22} and K_{33} are the elastic constants of deformation caused by splay, twist and bending, respectively. The parameters used in this work are: $K_{11} = 6.2 \times 10^{-12}\mathrm{N}$, $K_{22} = 3.6 \times 10^{-12}\mathrm{N}$ and $K_{33} = 8.25 \times 10^{-12}\mathrm{N}$ [28].

The surface anchoring energy F_s can be expressed as [28]:

$$F_S = -\frac{1}{2}W\int dS sin^2\Phi \tag{5}$$

where W is the anchoring energy coefficient of the liquid crystal molecules at the interface, and Φ is the angle between the LC director $(\hat{\mathrm{n}})$ and the preferred orientation of LC at the interface.

In order to describe the free energy of the system accurately, we introduce an additional term to the model, that is, interface free energy [28]:

$$F_\sigma = -\sigma\int dS \tag{6}$$

where σ is the interfacial tension that describes the effect of interfacial tension on the free energy of the system.

Hence, the total free energy contains two parts, one includes two terms related to interface energy $F_{\mathrm{A}} = F_{\mathrm{S}} + F_\sigma$, the other is consisted of volumetric energy $F_{\mathrm{v}} = F_{\mathrm{L}} + F_{\mathrm{E}}$. The total free energy is defined as:

$$F = F_{\mathrm{v}} + F_{\mathrm{A}} \tag{7}$$

It describes the imbalance of free energy of the system. The presence of GADs inside LCDs would narrow down the difference between the interface energy and the volumetric energy, thus the F.

4. Conclusion

We present a systematic study on controllable ingestion and release of aqueous phase (the external components) using 3D LCDs. The LC molecular alignment within a spherical droplet confinement can be well tuned via the interfacial anchoring conditions, thus forming various topological defects for guiding and trapping small colloids. The thermodynamic fluctuation at the LC-water interface with a strong perpendicular anchoring drives the formation of interfacial protrusions. As a result, the aqueous phase can intrude into the LCD in the forms of tiny GADs. The assembly of GADs exhibits obviously visible chains and clusters radially align along the spoke of the host LCD, forming configurational fractal structures. More importantly, the spontaneously ingested GADs can move with the point defect in the LCD and eventually be triggered to release by simply changing the anchoring conditions at the LC-water interface. The point defect in LCD and the elastic energy are therefore the key for the assembly and manipulation of GADs in a host LCD. Owing to the anisotropic interactions between GADs and surrounding LCs, we can create configurational fractal structures with high sophistication and flexibility. In particular, the order of the GADs assembly can be precisely controlled and manipulated by tuning the interfacial tension and the size of host LCDs. These phenomena have been confirmed both experimentally and in terms of a Landau–de Gennes based free energy calculation.

Such a reversible process of ingestion and release of aqueous phase via spherical LCDs happens in an all-fluidic medium. This proposed method is simple and achievable in a wide range of experimental parameters, and the use of droplet microfluidics enables the creation of monodisperse LCDs with tunable size and various components, revealing a route for constructing multi-compartmental hierarchical structures, and envisaging various potential applications such as artificial cells, drug and pharmaceutical nutrient delivery, food processing, and other soft matter-based microchemistries.

CRediT authorship contribution statement

Ruizhi Yang: Conceptualization, Investigation, Writing – original draft. **Yueming Deng:** Investigation, Validation. **Shuting Xie:** Investigation. **Mengjun Liu:** Investigation, Validation. **Yiying Zou:** Investigation. **Tiezheng Qian:** Writing – review & editing. **Qi An:** Investigation, Validation. **Jiamei Chen:** . **Shitao Shen:** . **Albert van den Berg:** Writing – review & editing. **Minmin Zhang:** Conceptualization, Resources, Writing – review & editing, Visualization, Supervision, Funding acquisition, Project administration. **Lingling Shui:** Conceptualization, Resources, Writing – review & editing, Visualization, Supervision, Funding acquisition, Project administration.

Declaration of Competing Interest

The authors declare that they have no known competing financial interests or personal relationships that could have appeared to influence the work reported in this paper.

Data availability

Data will be made available on request.

Acknowledgments

We appreciate the financial support from the Special project for marine economy development of Guangdong Province (GDNRC[2023] 26), the Key Project of National Natural Science Foundation of China (No. 12131010), Guangdong Province Basic and Applied Research Fund (2021A1515110236), and the Science and Technology Program of Guangzhou (202201010248). The International-Hong Kong-Macao-Taiwan Top Talents Exchange Program of Guangdong Province (No. 2022A0505020004), the 2022 Guangdong-Hong Kong-Macao Greater Bay Area Exchange Programs of SCNU, and the Young Scholar Foundation of South China Normal University (21KJ08). The fellowship of China Postdoctoral Science Foundation (2022M711224).

Appendix A. Supplementary material

Supplementary data to this article can be found online at https://doi.org/10.1016/j.jcis.2023.08.089.

References

[1] O. Staufer, F. Dietrich, R. Rimal, M. Schroeter, S. Fabritz, H. Boehm, S. Singh, M. Moeller, I. Platzman, J.P. Spatz, Bottom-up assembly of biomedical relevant fully synthetic extracellular vesicles, Sci. Adv. 7 (36) (2021) eabg6666, https://doi.org/10.1126/sciadv.abg6666.

[2] A. Zambrano, G. Fracasso, M. Gao, M. Ugrinic, D. Wang, D. Appelhans, A. deMello, T.Y.D. Tang, Programmable synthetic cell networks regulated by tuneable reaction rates, Nat. Commun. 13 (1) (2022) 3885, https://doi.org/10.1038/s41467-022-31471-5.

[3] S. Chen, J.G. Bomer, W.G. van der Wiel, E.T. Carlen, A. van den Berg, Top-down fabrication of Sub-30 nm monocrystalline silicon nanowires using conventional microfabrication, ACS Nano 3 (11) (2009) 3485–3492, https://doi.org/10.1021/nn901220g.

[4] M. Weiss, J.P. Frohnmayer, L.T. Benk, B. Haller, J.-W. Janiesch, T. Heitkamp, M. Borsch, R.B. Lira, R. Dimova, R. Lipowsky, E. Bodenschatz, J.-C. Baret, T. Vidakovic-Koch, K. Sundmacher, I. Platzman, J.P. Spatz, Sequential bottom-up assembly of mechanically stabilized synthetic cells by microfluidics, Nat. Mater. 17 (1) (2018) 89–96, https://doi.org/10.1038/nmat5005.

[5] J. Li, W.D. Jamieson, P. Dimitriou, W. Xu, P. Rohde, B. Martinac, M. Baker, B. W. Drinkwater, O.K. Castell, D.A. Barrow, Building programmable multicompartment artificial cells incorporating remotely activated protein channels using microfluidics and acoustic levitation, Nat. Commun. 13 (1) (2022) 4125, https://doi.org/10.1038/s41467-022-31898-w.

[6] S.R. Nagel, Experimental soft-matter science, Rev. Mod. Phys. 89 (2) (2017) 025002, doi:10.1103/RevModPhys.89.025002.

[7] A.S. Utada, E. Lorenceau, D.R. Link, P.D. Kaplan, H.A. Stone, D.A. Weitz, Monodisperse double emulsions generated from a microcapillary device, Science 308 (5721) (2005) 537–541, https://doi.org/10.1126/science.1109164.

[8] S.-H. Kim, D.A. Weitz, One-step emulsification of multiple concentric shells with capillary microfluidic devices, Angew. Chem.-Int. Ed. 50 (37) (2011) 8731–8734, https://doi.org/10.1002/anie.201102946.

[9] J.-W. Kim, S.H. Han, Y.H. Choi, W.M. Hamonangan, Y. Oh, S.-H. Kim, Recent advances in the microfluidic production of functional microcapsules by multiple-emulsion templating, Lab Chip 22 (12) (2022) 2259–2291, https://doi.org/10.1039/d2lc00196a.

[10] I. Musevic, M. Skarabot, U. Tkalec, M. Ravnik, S. Zumer, Two-dimensional nematic colloidal crystals self-assembled by topological defects, Science 313 (5789) (2006) 954–958, https://doi.org/10.1126/science.1129660.

[11] N.V. Solodkov, J.-U. Shim, J.C. Jones, Self-assembly of fractal liquid crystal colloids, Nat. Commun. 10 (2019) 198, https://doi.org/10.1038/s41467-018-08210-w.

[12] J.K. Guo, S.H. Hong, H.J. Yoon, G. Babakhanova, O.D. Lavrentovich, J.K. Song, Laser-induced nanodroplet injection and reconfigurable double emulsions with designed inner structures, Adv. Sci. (Weinh) 6 (17) (2019) 1900785, https://doi.org/10.1002/advs.201900785.

[13] L. Schoonen, J.C.M. van Hest, Compartmentalization approaches in soft matter science: From nanoreactor development to organelle mimics, Adv. Mater. 28 (6) (2016) 1109–1128, https://doi.org/10.1002/adma.201502389.

[14] T. Turiv, R. Koizumi, K. Thijssen, M.M. Genkin, H. Yu, C. Peng, Q.-H. Wei, J. M. Yeomans, I.S. Aranson, A. Doostmohammadi, O.D. Lavrentovich, Polar jets of swimming bacteria condensed by a patterned liquid crystal, Nat. Phys. 16 (4) (2020) 481–487, https://doi.org/10.1038/s41567-020-0793-0.

[15] L. Mei, M. Jin, S. Xie, Z. Yan, X. Wang, G. Zhou, A. van den Berg, L. Shui, A simple capillary-based open microfluidic device for size on-demand high-throughput droplet/bubble/microcapsule generation, Lab Chip 18 (18) (2018) 2806–2815, https://doi.org/10.1039/c8lc00479j.

[16] J.M. Brake, M.K. Daschner, Y.Y. Luk, N.L. Abbott, Biomolecular interactions at phospholipid-decorated surfaces of liquid crystals, Science 302 (5653) (2003) 2094–2097, https://doi.org/10.1126/science.1091749.

[17] J.N. Lsraelachvili, Third Edition Intermolecular and Surface Forces, 2nd ed., Academic Press, London, 1991.

[18] D.G. Kotsifaki, S.N. Chormaic, Plasmonic optical tweezers based on nanostructures: fundamentals, advances and prospects, Nanophotonics 8 (7) (2019) 1227–1245, https://doi.org/10.1515/nanoph-2019-0151.

[19] Y.-H. Tseng, A. Prosperetti, Local interfacial stability near a zero vorticity point, J. Fluid Mech. 776 (2015) 5–36, https://doi.org/10.1017/jfm.2015.246.

[20] J.C. Loudet, P. Barois, P. Poulin, Colloidal ordering from phase separation in a liquid-crystalline continuous phase, Nature 407 (6804) (2000) 611–613, https://doi.org/10.1038/35036539.

[21] F.Y. Deng, L.L. Liu, Z. Li, J.C. Liu, 3D printed Ti6Al4V bone scaffolds with different pore structure effects on bone ingrowth, J. Biol. Eng. 15 (1) (2021) 4, https://doi.org/10.1186/s13036-021-00255-8.

[22] C. Peng, T. Turiv, Y. Guo, S.V. Shiyanovskii, Q.-H. Wei, O.D. Lavrentovich, Control of colloidal placement by modulated molecular orientation in nematic cells, Sci, Adv 2 (9) (2016), e1600932, https://doi.org/10.1126/sciadv.1600932.

[23] M. Ravnik, S. Žumer, Landau–de Gennes modelling of nematic liquid crystal colloids, Liq. Cryst. 36 (10–11) (2009) 1201–1214, https://doi.org/10.1080/02678290903056095.

[24] Y.-K. Kim, X. Wang, P. Mondkar, E. Bukusoglu, N.L. Abbott, Self-reporting and self-regulating liquid crystals, Nature 557 (7706) (2018) 539–544, https://doi.org/10.1038/s41586-018-0098-y.

[25] P. Beyazkilic, S. Akcimen, C. Elbuken, B. Ortaç, S. Cai, E. Bukusoglu, Contactless pulsed and continuous microdroplet release using photothermal liquid crystals, Adv. Funct. Mater. 32 (44) (2022) 2205385.

[26] J. Shechter, N. Atzin, A. Mozaffari, R. Zhang, Y. Zhou, B. Strain, L.M. Oster, J.J. de Pablo, J.L. Ross, Direct observation of liquid crystal droplet configurational transitions using optical tweezers, Langmuir 36 (25) (2020) 7074–7082, https://doi.org/10.1021/acs.langmuir.9b03629.

[27] B.X. Li, R.L. Xiao, S. Paladugu, S.V. Shiyanovskii, O.D. Lavrentovich, Three-dimensional solitary waves with electrically tunable direction of propagation in nematics, Nat. Commun. 10 (1) (2019) 3749, https://doi.org/10.1038/s41467-019-11768-8.

[28] W.S. Wei, Y. Xia, S. Ettinger, S. Yang, A.G. Yodh, Molecular heterogeneity drives reconfigurable nematic liquid crystal drops, Nature 576 (7787) (2019) 433–436, https://doi.org/10.1038/s41586-019-1809-8.